A Scatterer Localization Method Using Large-Scale Antenna Array Systems

Zhang, Guojin; Cai, Xuesong; Nielsen, Jesper Odum; Pedersen, Gert Frolund; Tufvesson, Fredrik

Published in:
2022 IEEE Conference on Antenna Measurements & Applications

2022

Document Version:
Peer reviewed version (aka post-print)

A Scatterer Localization Method Using Large-Scale Antenna Array Systems

Guojin Zhang*, Xuesong Cai†, Jesper Ødum Nielsen*, Gert Frølund Pedersen* and Fredrik Tufvesson†
*Department of Electronic Systems, Aalborg University, Aalborg, Denmark
†Department of Electrical and Information Technology, Lund University, Lund, Sweden
Email: *guojin@es.aau.dk, †xuesong.cai@eit.lth.se, *jni@es.aau.dk, *gfp@es.aau.dk †fredrik.tufvesson@eit.lth.se
Corresponding author: Xuesong Cai

***Abstract*—As ultra-massive multiple-input multiple-output (UM-MIMO) has emerged as a key technology for millimeter-wave and terahertz communications, the spherical wave propagation should be considered for channel modeling. Therefore, it is critical to identify the locations and evolving behaviors of scatterers, i.e., the sources of the spherical wavefronts. In this contribution, a novel space-alternating generalized expectation-maximization (SAGE) based scatterer localization algorithm is proposed, where a large-scale antenna array is divided into multiple sub-arrays. Due to the decreased aperture of each sub-array, plane wave assumption can be applied to estimate the angles of departure/arrival, delays and amplitudes of multipath components (MPCs). Based on the angle variations of MPCs observed at different sub-arrays, the corresponding scatterers can be located. The proposed algorithm is verified in a simulation using a large-scale uniform circular array (UCA) system. Moreover, we apply this algorithm to an indoor measurement campaign conducted at 27-29 GHz in a hall scenario. Dominant scatterers are identified, which can be used for the development of further geometry-based stochastic channel models.**

***Index Terms*—Large-scale antenna array, spherical wave propagation, scatterer localization, channel parameter estimation.**

I. Introduction

To establish realistic geometry-based stochastic channel models for ultra-massive multiple-input multiple-output (UM-MIMO) communications, it is necessary to consider spherical wave propagation [1]–[3]. In [4]–[6], under spherical wavefront assumption, propagation delays, angles of departure or arrival (AoD or AoA), amplitudes, and the distances from the array to the first or last hop scatterers of the multipath components (MPCs) are estimated using a whole large-scale antenna array. The locations of the scatterers were estimated by checking the distance and angular information. As the distances between the array and the first or last hop scatterers have to be considered in the estimation, it leads to high computational complexities. To decrease the complexity of the estimation algorithm, a novel scatterer localization method is proposed in this contribution, where a large-scale antenna array is divided into multiple sub-arrays, to make it feasible to estimate the parameters of the MPCs under the plane wave assumption. According to the estimated angles of MPCs observed at each sub-arrays, the corresponding locations of the scatterers can be estimated.

The performance of the proposed scatterer localization algorithm is verified by a simulation with a large-scale uniform circular array (UCA). Furthermore, the proposed algorithm is applied to a measurement campaign conducted in an indoor hall scenario at 27-29 GHz. Eleven consecutive elements are formed as a sub-array moving across the UCA. Due to the narrow beamwidths of the transmitter (Tx) and receiver (Rx) biconical antennas in elevation domain and that they were placed with the same height, we do not consider elevations in our estimation. The parameters, i.e., the delays, azimuths and amplitudes of the MPCs observed at each sub-array, are independently estimated using the space-alternating generalized expectation-maximization (SAGE) algorithm [7] under the plane wave assumption. Based on the azimuths of MPCs estimated at different sub-arrays, the scatterers are located using an iterative non-linear least squares algorithm, i.e. the Levenberg and Marquard algorithm [8]. The performance of the proposed scatterer localization method is verified by mapping the estimated scatterers to the real physical objects in the indoor hall scenario. Moreover, with the estimated parameters obtained from each sub-array across the whole UCA, the spatial non-stationary for the large-scale array can also be observed.

The rest of the paper is organized as follows. Sect. II presents the signal model and the proposed scatterer localization algorithm. In Sect. III, simulation results in a line-of-sight (LoS) scenario are elaborated to evaluate the performance of the proposed algorithm. Moreover, the measurement campaign conducted in the indoor hall scenario and measurement-based estimation results are presented in Sect. IV. Finally, conclusive remarks are included in Sect. V.

II. Signal model and scatterer localization

To apply the SAGE algorithm with the plane wavefront assumption, let us consider a UCA with M elements that is divided into multiple sliding sub-arrays as shown in Fig. 1. The mth sub-array contains P elements with its center as the mth element of the UCA, resulting in a total number of M sub-arrays. The UCA with a radius r is located in the x-y-z plane, with its center as the origin. The mth sub-array is located in its local x_m-y_m-z_m plane, with the center of the sub-array as the origin. The angle between x and x_m is $\vartheta_m = \frac{2\pi m}{M}$. A finite number of L_m plane waves are assumed to impinge

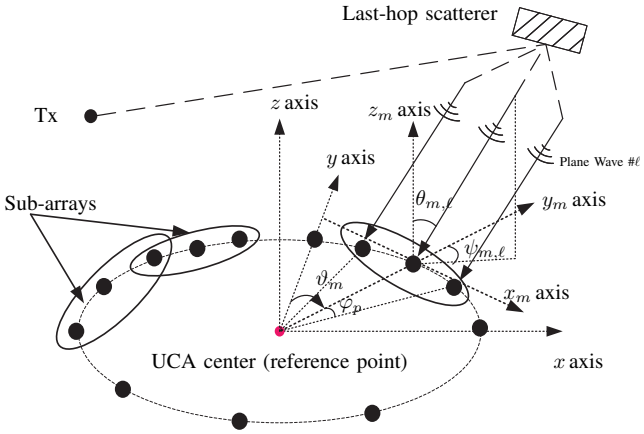

Fig. 1: Sub-arrays moving across the UCA.

into the mth sub-array. in the x_m-y_m-z_m coordinate system, the complex amplitude, delay, azimuth and elevation of the ℓth path that impinges into the mth sub-array are denoted as $\alpha_{m,\ell}$, $\tau_{m,\ell}$, $\psi_{m,\ell}$, $\theta_{m,\ell}$, respectively. The direction vector $\mathbf{\Omega}_{m,\ell}$ can be written as

$$\mathbf{\Omega}_{m,\ell} = [\sin\theta_{m,\ell}\sin\psi_{m,\ell},\ \sin\theta_{m,\ell}\cos\psi_{m,\ell},\ \sin\theta_{m,\ell}]^T. \quad (1)$$

The coordinate $\mathbf{S}_{m,p}$ of the pth array element of the mth sub-array in the x_m-y_m-z_m system can be written as

$$\mathbf{S}_{m,p} = [r\sin\varphi_p,\ -r + r\cos\varphi_p,\ 0]^T \quad (2)$$

where φ_p denotes the angle between the pth array element and the center of the sub-array. The channel transfer functions $\mathbf{H}_{m,\ell}(\mathbf{f})$ of the ℓth path at the reference point (the center of the mth sub-array) in the frequency range $\mathbf{f}$ can be described as

$$\mathbf{H}_{m,\ell}(\mathbf{f}) = \alpha_{m,\ell}e^{-j2\pi\mathbf{f}\tau_{m,\ell}} \quad (3)$$

where $\mathbf{f} = [f_1, \ldots, f_N]$ contains N frequency points that sweep the bandwidth of interest. Due to the propagation distance difference between the reference point and the pth element, the frequency response $\mathbf{H}^p_{m,\ell}(\mathbf{f})$ at the pth element can be described as

$$\mathbf{H}^p_{m,\ell}(\mathbf{f}) = \mathbf{H}_{m,\ell}(\mathbf{f}) \odot e^{j2\pi\mathbf{f}(\frac{\mathbf{\Omega}_{m,\ell}\cdot\mathbf{S}^T_{m,p}}{c})} \quad (4)$$

where c is the speed of light and $\odot$ means the element-wise product. The signal $\mathbf{H}(\mathbf{f};\mathbf{\Psi}_{m,\ell})$ contributed by the ℓth path for the mth sub-array can be described as

$$\mathbf{H}_m(\mathbf{f};\mathbf{\Psi}_{m,\ell}) = [\mathbf{H}^1_{m,\ell}, \ldots, \mathbf{H}^P_{m,\ell}]^T. \quad (5)$$

The output of the mth sub-array contributed by all the L_m MPCs can be written as

$$\mathbf{H}_m(\mathbf{f};\mathbf{\Psi}_m) = \sum_{\ell=1}^{L_m}\mathbf{H}_m(\mathbf{f};\mathbf{\Psi}_{m,\ell}) + \mathbf{N}(\mathbf{f}) \quad (6)$$

where $\mathbf{N}(\mathbf{f})$ denotes complex Gaussian noise. With the signal model above, the SAGE algorithm is applied independently to estimate the propagation parameter set $\mathbf{\Psi}_m = [\alpha_{m,\ell}, \tau_{m,\ell}, \psi_{m,\ell}, \theta_{m,\ell}; \ell = 1, \ldots, L_m]$ of the MPCs for the mth sub-array in the x_m-y_m coordinate system[1].

Based on the SAGE estimation results, a multipath-component-distance (MCD) threshold method [9] is applied to associate the estimated paths at different sub-arrays using their delay and angular information, since the same path could experience death-birth behaviour across the large aperture of the whole array. Note that the estimated azimuth angle $\hat{\psi}_{m,\ell}$ in the local coordinate system is converted to the angle $\hat{\phi}_{m,\ell}$ in the global system as $\hat{\phi}_{m,\ell} = \hat{\psi}_{m,\ell} + \vartheta_m$ for path association/tracking. Based on the path tracking results (e.g., as shown in Fig. 5), the locations of scatterers are obtained using an iterative non-linear least squares algorithm, i.e. the Levenberg and Marquard algorithm [8] as follows.

For an associated path with its azimuths and elevations at different sub-arrays estimated as $\hat{\phi}_{m,\ell}$ and $\hat{\theta}_{m,\ell}$, let us denote the location of the corresponding scatterer in x-y-z system as $\mathbf{V}_\ell$. The location vector of sub-array centers is known as $\mathbf{R}_m$. Then, in x-y-z system the ground-truth unit vector of the direction of arrival $\mathbf{\Theta}_{m,\ell}$ of the ℓth path observed at the mth sub-array can be calculated as

$$\mathbf{\Theta}_{m,\ell} = \frac{\mathbf{V}_\ell - \mathbf{R}_m}{\|\mathbf{V}_\ell - \mathbf{R}_m\|} \quad (7)$$

The unknown location $\mathbf{V}_\ell$ can be obtained by minimizing the cost function

$$c(\mathbf{V}_\ell) = \Sigma_m(\hat{\mathbf{\Theta}}_{m,\ell} - \mathbf{\Theta}_{m,\ell})^T(\hat{\mathbf{\Theta}}_{m,\ell} - \mathbf{\Theta}_{m,\ell}) \quad (8)$$

as

$$\hat{\mathbf{V}}_\ell = \arg\min_{\mathbf{V}_\ell} c(\mathbf{V}_\ell) \quad (9)$$

where $\hat{\mathbf{\Theta}}_{m,\ell}$ is the estimated direction vector of arrival according to $\hat{\phi}_{m,\ell}$ and $\hat{\theta}_{m,\ell}$.

III. Simulation

To evaluate the performance of the proposed scatterer localization algorithm, a simulation of a LoS scenario is considered. A UCA is used as the Rx side, and a single antenna as the Tx side. The radius of the UCA is set as 0.24 m. The distance between Tx and the UCA center is set as 3.75 m. The delay, azimuth, elevation, and amplitude of incident wave towards the center of the UCA are set as 12.5 ns, 40 °, 90 ° and 1, respectively. In the simulations, both P=3 and P=11 are considered to investigate the effect of sub-array sizes. Moreover, signal-to-noise ratios (SNRs) of 30 dB and infinite (i.e., no noise) are considered. The estimated azimuths $\hat{\psi}_{m,\ell}$ in local coordinate system and azimuths $\hat{\phi}_{m,\ell}$ in global system obtained at each sub-array are shown in Fig. 2(a) and Fig. 2(b). In Fig. 2(a), it can be observed that the estimated azimuth $\hat{\psi}_{m,\ell}$ decreases 1° as the center of the sub-array moves one element, which is reasonable according to the geometry. It can also be observed that the trajectory of azimuths $\hat{\phi}_{m,\ell}$ is a sine-alike shape in Fig. 2(b), which is caused by the near-field effect as expected. Significant fluctuations of estimated azimuths are

[1] As mentioned earlier, we consider 2D transmission in this paper. However, to generalize the signal model, we have elevation angels throughout this section.

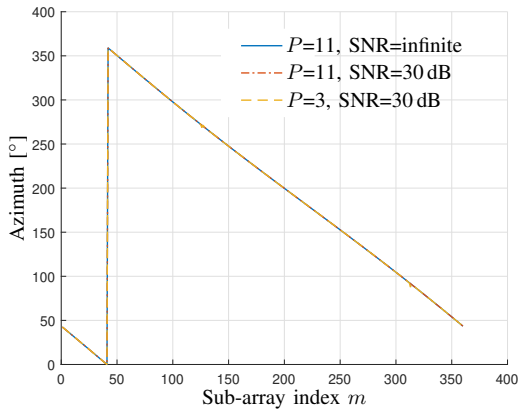

(a)

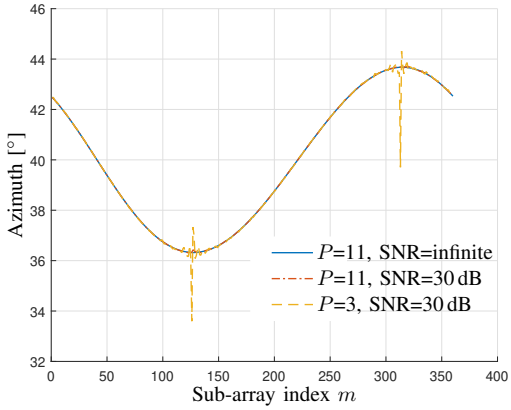

(b)

Fig. 2: The estimated azimuths $\hat{\psi}_{m,\ell}$ and azimuths $\hat{\phi}_{m,\ell}$ obtained at each sub-array in the simulation. (a) Estimated azimuths $\hat{\psi}_{m,\ell}$ in local coordinate system. (b) Estimated azimuths $\hat{\phi}_{m,\ell}$ in global system.

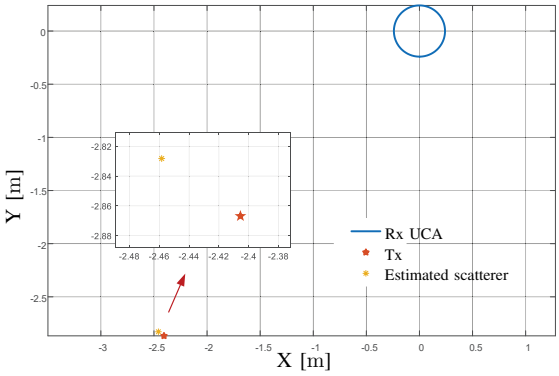

Fig. 3: Simulation with noise data for the scatterer localization of LoS scenario.

observed in the noisy situation. It is caused by the fact that the accuracy of angular estimation decreases, as the direction of the incident waves are parallel to the sub-array, leading to larger estimation error. Moreover, it can be found that the estimation accuracy is significantly affected by the noise, especially with a smaller number of elements within each sub-array. Considering the Rayleigh distance, the number of the

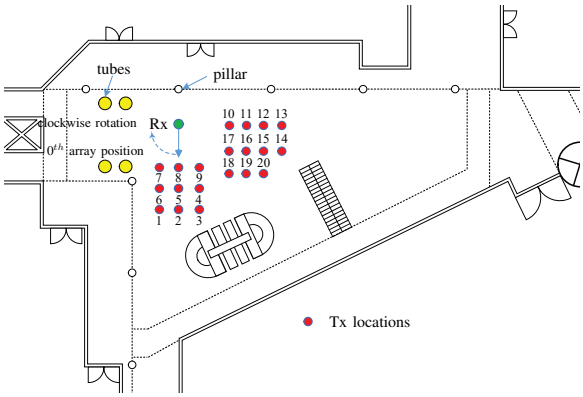

Fig. 4: The top-view of the hall scenario.

elements within a sub-array should be less than nineteen, if the nearest scatter is two meters away. Therefore, to balance the accuracy of the estimation and effects of the near field, eleven consecutive virtual elements are practically chosen as a sub-array for the scatterer localization. According to the azimuths $\hat{\phi}_{m,\ell}$ in global system and the location of each sub-array, the location of the last hop scatterer (Tx antenna position here) is estimated as shown in Fig. 3. The distance errors between the estimated scatterer and Tx antenna are 0.0655 m and 0.0654 m, in the noisy and noise free cases, respectively. One may expect that the estimation accuracy should be zero in the noise free situation. In fact, the non-zero error is because of the model mismatch herein. In other words, when the scattterer is too near to the sub-array (e.g., as shown in this simulation), near field propagation still exist. Therefore, in our future work, we will investigate the suitable number of antennas used in one sub-array more comprehensively.

IV. Measurement

A measurement campaign was conducted in an indoor hall scenario at 27-29 GHz as illustrated in Fig. 4. A vector network analyzer (VNA)-based channel sounder [10] was used to collect channel transfer functions. Four yellow ventilation tubes (marked as yellow circles) and six white pillars (marked as white circles) are located in the hall scenario. The shape of the hall is irregular and the dimension is approximately $39\times20\times10$ m^3. A commercial biconical antenna SZ-2003000/P [11] and a homemade biconical antenna [12] were utilized as the Tx and Rx antennas, respectively. The heights of the Tx and Rx antennas are both 1.50 m. A total of 20 snapshots were recorded by moving the Tx antenna 1 m apart. For each Tx position, the Rx antenna was rotated clockwise to form a large-scale UCA with a radius of r=0.24 m. For each snapshot, N=750 frequency points were swept. M=360 UCA elements were collected by the VNA.

Using the SAGE algorithm and the MCD threshold tracking method, the examples of the tracking results in delay and angular domain obtained from the measurement at Tx position 5 are shown in Fig. 5(a) and Fig. 5(b), respectively. The spatial non-stationary across the elements of the large-scale array can be observed. The locations of the last hop scatterers are estimated as shown in Fig. 6, which shows a good match

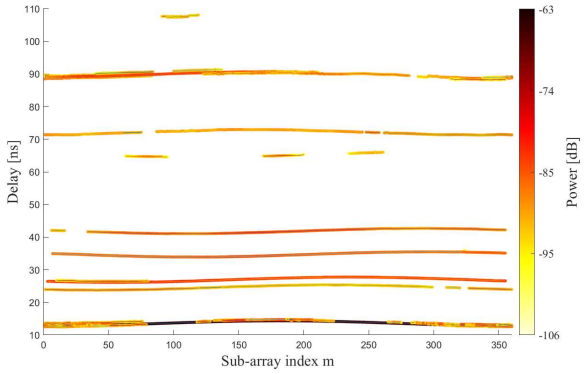

(a)

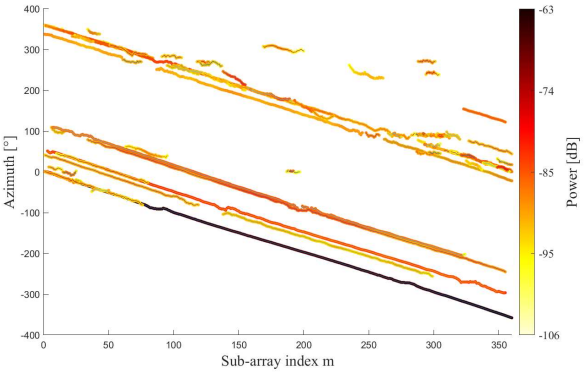

(b)

Fig. 5: Path tracking/association results in the measurement campaign. (a) Delay domain. (b) Azimuth domain.

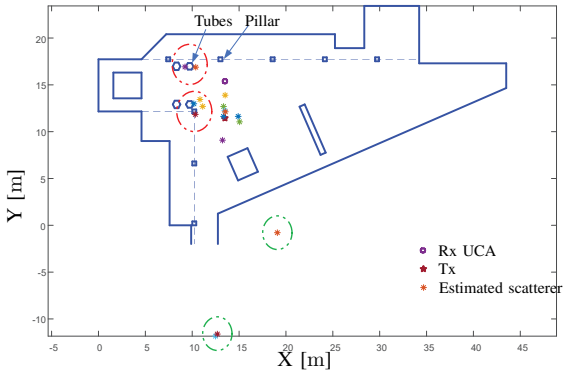

Fig. 6: The map of the hall scenario with physical objects and the estimated last hop scatterers obtained from the measurements.

with actual physical objects. For example, some scatterers (highlighted by red circles) are identified closely around the tubes and the pillars. Furthermore, it is also observed that some scatterers (highlighted by green circles) are located outside the hall, which are called "virtual scatterers". These scatterers are probably due to specular reflections from smooth surfaces, resulting in the mirror positions of Tx.

V. Conclusions

A novel space-alternating generalized expectation-maximization (SAGE) based scatterer localization algorithm is proposed. The large-scale antenna array is divided into multiple sub-arrays. Plane wave propagation parameters, i.e., amplitudes, delays and directions of departure/arrival, of the multipath components (MPCs) impinging to each sub-array are estimated independently using the SAGE algorithm. Using the estimated angles and the locations of each sub-array, the locations of scatterers can be estimated. The performance of the proposed algorithm is verified in the simulation. Moreover, the estimated scatterers in the measurement campaign shows consistency to the actually physical objects. Future work will investigate the optimal number of antennas in a sub-array, and establish scatterer-based channel models. Moreover, computational complexity of the proposed algorithm will be compared with that of the method using the entire array under spherical-wave assumption.

VI. Acknowledgements

This work has been partly funded by the strategic research area ELLIIT, Excellence Center at Linköping – Lund in Information Technology, and Ericsson. The work of Xuesong Cai is also supported by the Horizon Europe Framework Programme under the Marie Skłodowska-Curie grant agreement No. 101059091.

References

[1] X. Cai and W. Fan, "A Complexity-Efficient High Resolution Propagation Parameter Estimation Algorithm for Ultra-Wideband Large-Scale Uniform Circular Array," *IEEE Transactions on Communications*, vol. 67, no. 8, pp. 5862–5874, Aug 2019.

[2] Y. Ji, W. Fan, and G. F. Pedersen, "Near-Field Signal Model for Large-Scale Uniform Circular Array and Its Experimental Validation," *IEEE Antennas and Wireless Propagation Letters*, vol. 16, pp. 1237–1240, 2017.

[3] X. Cai, W. Fan, X. Yin, and G. F. Pedersen, "Trajectory-Aided Maximum-Likelihood Algorithm for Channel Parameter Estimation in Ultrawideband Large-Scale Arrays," *IEEE Transactions on Antennas and Propagation*, vol. 68, no. 10, pp. 7131–7143, 2020.

[4] X. Yin, S. Wang, N. Zhang, and B. Ai, "Scatterer Localization Using Large-Scale Antenna Arrays Based on a Spherical Wave-Front Parametric Model," *IEEE Transactions on Wireless Communications*, vol. 16, no. 10, pp. 6543–6556, Oct 2017.

[5] J. Chen, S. Wang, and X. Yin, "A Spherical-Wavefront-Based Scatterer Localization Algorithm Using Large-Scale Antenna Arrays," *IEEE Communications Letters*, vol. 20, no. 9, pp. 1796–1799, Sept 2016.

[6] Y. Ji, J. Hejselbæk, W. Fan, and G. F. Pedersen, "A Map-Free Indoor Localization Method Using Ultrawideband Large-Scale Array Systems," *IEEE Antennas and Wireless Propagation Letters*, vol. 17, no. 9, pp. 1682–1686, 2018.

[7] B. H. Fleury, M. Tschudin, R. Heddergott, D. Dahlhaus, and K. I. Pedersen, "Channel Parameter Estimation in Mobile Radio Environments Using the SAGE Algorithm," *IEEE Journal on Selected Areas in Communications*, vol. 17, no. 3, pp. 434–450, Mar 1999.

[8] M. Schmidhammer, C. Gentner, and B. Siebler, "Localization of Discrete Mobile Scatterers in Vehicular Environments Using Delay Estimates," in *2019 International Conference on Localization and GNSS (ICL-GNSS)*, 2019, pp. 1–6.

[9] X. Cai, G. Zhang, C. Zhang, W. Fan, J. Li, and G. F. Pedersen, "Dynamic Channel Modeling for Indoor Millimeter-Wave Propagation Channels Based on Measurements," *IEEE Transactions on Communications*, vol. 68, no. 9, pp. 5878–5891, 2020.

[10] J. Hejselbaek, W. Fan, and G. F. Pedersen, "Ultrawideband VNA based channel sounding system for centimetre and millimetre wave bands," in *2016 IEEE 27th Annual International Symposium on Personal, Indoor, and Mobile Radio Communications (PIMRC)*, 2016, pp. 1–6.

[11] "LB-SJ-180400-KF Datasheet," Tech. Rep. [Online]. Available: http://www.ainfoinc.com.cn/en/pro_pdf/new_products/antenna/Dual%20Polarization%20Horn%20Antenna/tr_LB-SJ-180400.pdf

[12] S. S. Zhekov, A. Tatomirescu, and G. F. Pedersen, "Antenna for Ultrawideband Channel Sounding," *IEEE Antennas and Wireless Propagation Letters*, vol. 16, pp. 692–695, 2017.